Enhancing Power Balancing and Fault Interruption in an Autonomous Smart Microgrid Design

KRISHA GRACE VALLEJOS, ELIJAH FERNANDEZ, ALLYSSA LARKIN, DAVID CABRERA, OMAR REYES DIAZ, AUSTIN VALLE, ALAN VU, TONY YIM, OMAR ALJUMAA, ANDREW SIERRA, MIGUEL ALCALA, NICK GARCIA, TOM BAILEY, STEVEN YAU, HA THU LE

Department of Electrical and Computer Engineering
California State Polytechnic University, Pomona
Pomona City, California 91768
UNITED STATES OF AMERICA

Abstract – In this study, a load balancing scheme and a fault interruption system are developed and implemented to improve an autonomous microgrid design. These features are needed to make the microgrid design better where supply-demand is balanced to ensure satisfactory voltages and fault situations are properly handled for the microgrid safety. The enhanced microgrid is implemented using MATLAB Simulink. Testing results have shown that the microgrid control system works properly and can handle various operational situations. The load balancing scheme is effective in matching power supply with load demand using different power sources (solar PV, battery, diesel generator). Voltage levels of both residential and commercial loads are maintained within ±5% tolerance of their respective nominal values. The fault interruption system operates properly and is effective in dealing with different faulty conditions. It successfully clears non-permanent faults and isolates a permanent fault. Overall, the original microgrid has been improved to be more autonomous as it can deal with more diverse operational conditions. The study outcomes contribute to expansion of smart microgrids by developing theoretical advanced features for real-world implementation of autonomous intelligent microgrids, which, in turn, make larger grids more dependable.

Keywords – Battery, control system, fault interruption, inverter, microgrid, power balancing, relay, solar PV.
Received: May 21, 2021. Revised: June 17, 2022. Accepted: July 15, 2022. Published: August 31, 2022.

1. Introduction

Microgrids are key components for making power grids more reliable, efficient, and smart. They can operate in interconnection with or independent from main power grids, where they provide power to isolated or remote areas. In case of an emergency that causes the main grids to be down, areas supported by microgrids will not be affected and can continue to receive power without interruption. This aspect is important for facilities such as hospitals or buildings that provide critical services.

This research focuses on improving a microgrid design that is called "original" microgrid in [1]. It is an autonomous microgrid that can operate independently from the main power system, thanks to a solar PV system, a battery, a diesel generator, a control system and supporting equipment. The microgrid design is based on Southern California El Monte city and implemented in MATLAB Simulink. The microgrid details are presented in Section 2.

The features to be improved include supply-demand balancing (i.e. power balancing) and fault interruption capability. These features are necessary because they ensure satisfactory grid voltages by

ensuring supply-demand balancing in more diverse situations while dealing with faulty conditions for the microgrid safety. The following section discusses the features to be improved, along with relevant literature.

Information for developing the advanced microgrid is obtained from a number of previous studies. Using data from small areas that rely on energy from diesel generators to test ways for transitioning to renewable energy, the research in [2] showed by simulation that it was able to generate a sufficient amount of power necessary to sustain 200 homes, 20 stores, and a general hospital through the use of solar and wind energy [2]. Simulations of wind energy in microgrids are possible using models in [3, 4].

Renewable energy resources like solar PV systems are becoming more obtainable for their low economical cost [5]. However, high outputs of PV systems leads to power quality issues such as the reverse of power flow in line feeders, overvoltage, and voltage unbalance [5] [6]. An overvoltage due to high PV generation is a likely scenario in the El Monte region which has lots of sunshine year round. The original microgrid contains a PV system that is designed to work properly under a certain voltage threshold [1].

In the event that the PV system generates more power than required while the load demand is low, it can lead towards power quality issues in the distribution network system such as voltage rises and unbalanced voltages. This justifies the need to implement a power and load balancing scheme for the original microgrid. It aims to ensure acceptable supply-load balance, keep voltages within acceptable limits and avoid overvoltage and undervoltage conditions.

Previous studies suggest various methods to implement overvoltage mitigation, including on-load tap-changers, reduction of line impedances, use of electric vehicle charging stations as dummy loads, and reactive power absorption [7]. The strategies in the literature that our study considered include active power curtailment (APC) and dynamic electrical array reconfiguration (EAR) for solar modularization, and dynamic demand response using a dummy load.

The use of active power adjustments is a consideration to the system not only to recover transient stability but also as a possibility to reach stability quicker [8]. APC, also called ramp-rate control, is mentioned as a viable overvoltage protection technique in the literature [9-11]. It is used to control upward power fluctuations by "adjusting the actual operating point of the PV converter below its maximum power point (MPP)" [9]. Case studies simulating APC algorithms in [9] have also found that combining the use of battery energy storage (BES) or hybrid energy storage systems (HESS) with APC is economical by reducing the battery capacity and energy losses, and overall prolonging the battery life. Partial shading conditions are common concerns in solar panel efficiency, and mitigation techniques have been extensively researched in [10] [12-14].

Neither APC nor EAR techniques align exactly with our study goal involving the power balancing scheme. Indeed, APC is intended for overvoltage mitigation, and EAR utilizes dynamic array switching. However, they both focus on the initial "pre-processing" of irradiance levels by influencing MPP-tracking (MPPT) inverter controller readings. Instead, our study proposes a novel utilization of dynamic array configuration for the purpose of overvoltage mitigation in the particular case that APC either fails or is not implemented in the solar system. We aim to improve the original microgrid control logic (i.e. increasing its complexity) to dynamically disconnect and reconnect solar modules as needed to mitigate overvoltage scenarios.

Dummy loads have been integrated into microgrids as an outlet for excess power that the solar panels may produce, and have been shown in the literature to be a common method for overvoltage protection [7]. The use of dummy loads gives the microgrids an additional tool to store excess power, beyond their main energy storage system capability [15]. A project with the integration of dummy loads was conducted at the Akagi of the Central Research Institute of Electric Power Industry in Japan. The project utilized a 200-kVA dummy load connected to three 100- kW inverters [16]. Through the use of dummy loads, microgrids are able to become more efficient while improving their voltage conditions. The original microgrid did not consider the potential excess energy that may be produced, thus leading to the potential of overvoltage. Therefore, our study considers adding a

dummy load to the original microgrid to store excess solar power, help mitigate overvoltage conditions and enhance supply-demand balance.

Apart from using dummy loads, we also considered the use of a Static Var Compensator (SVC) to control microgrid voltage. SVCs are used to dynamically compensate reactive power [17]. Implementing SVCs into a microgrid can help reduce system losses and deal with extended voltage outage conditions [18] [19]. Ultimately, we have decided not to implement a SVC in our enhanced microgrid based on further investigation, as explained later.

Apart from power balancing and voltage control, fault protection is a vital component for all power systems. A fault is defined as a surge of current when the current deviates from its intended path. When dealing with faults in the utility system, the main goal is to quickly isolate the fault to minimize its impact. Such faults in a power system can be characterized as three-line-to-ground (3L2G), single-line-to-ground (SLG), or line-to-line. Faults vary in occurrence and severity with a three-phase fault to be the most severe, but less common compared to SLG faults [20]. Key devices for isolating faults are circuit breakers that are utilized to interrupt a fault current based on relay logic that monitor various aspects of the power system that may include impedance, voltage, and current.

Fault protection has been investigated in various studies. A research team at the University of Santa Maria researched a recloser-fuse coordination protection methodology for distributed generation systems using Gate Turn-Off Thyristors (GTO). The team referenced other research that used a computer program to simulate faults and if using recloser-fuse coordination, sensors, and GTO thyristors would be able to mitigate these faults. They determined that, with proper placement of reclosers and GTO thyristors in an electrical distribution system, utilities should be able to provide uninterrupted and reliable power for most portions of a feeder [21].

Looking more closely at reclosers, we see that there is an important parameter to be analyzed. It is the dead time. Dead time is the time interval from opening the circuit line to closing it to check for fault currents. While the dead time can be determined by standards some researchers wanted to explore the idea of a more adaptable dead time. These researchers used an algorithm that used waveform patterns of transient voltages. They used this transient voltage data, fed it into an algorithm, then implemented all this by using MODELS and the electromagnetic transient program (EMTP). The algorithm then calculates ideal dead times based on individual events. The researchers found that setting dead times to be more variable and tailoring them to specific circuits and events could lead to more successful reclosing events, reduced outage times, and less equipment damage [22, 23].

The idea of reclosers was such an attractive one, a utility company in Ireland performed a trial on them. The Electric Supply Board (ESB) wanted to discover different methods that would be able to mitigate and lower the number of power outages to customers and they decided to try reclosers. The methodology was to install thirteen 10kV and sixteen 20kV rated reclosers in carefully chosen areas throughout their electrical grid. After months of use the researchers would collect the data from all reclosers and analyze them individually. The main results the researchers obtained were that reclosers were expected to operate in the field successfully and installing them in decisive locations would cover the cost of investments [24].

In the original microgrid design, circuit breakers were modeled, but they were solely operated by the control logic to only switch between various generator sources. A protective system was not in place which made the microgrid susceptible to potential dangers such as severe weather conditions, fallen trees, car crashes, etc. In downtown El Monte, these concerns are a real possibility. The need for a new fault protection system was critical. To address this problem, we aim to design and implement a fault interruption system using knowledge from the previously mentioned research. We incorporate the fault interruption system into the original microgrid by utilizing reclosers with appropriate deadtimes in certain areas of the microgrid.

Reinstating all of the above discussions, the main objective of this study is to enhance the viability of the original smart autonomous microgrid through the two following methods:

a) Balancing supply-load and mitigating overvoltage conditions via enhancing the control logic, incorporating a dummy load, and modularizing the solar PV system.

b) Incorporating protective capability via designing and implementing a fault interruption system that employs two-fast and two-slow relay switching scheme.

2. Description of original microgrid

2.1 Load modeling using real-world data

The original microgrid design was based on the downtown area of El Monte city, California. It supplies power to a small community of 176 residential homes and 37 commercial buildings that include schools, a hospital, courthouse, churches, and so on. Using data from the U.S Energy Information Administration and energy reports from Southern California Edison, a large power utility, the microgrid Annual Energy, Average Energy Per Month, Average Energy Per Day, and Average Real Power per Day were calculated [1].

Because the area of El Monte is near Los Angeles, data from Los Angeles Department of Water and Power were used to model the hourly load demand for El Monte for an entire year. This means that El Monte would have the highest power demand in June with 1837.9kW and an average power consumption per day of 786.24kW. All residential loads are assumed to have a peak real power demand of 4kW, which is a typical demand for an American single family house. A power factor of 0.9 lagging is applied to the entire load of the microgrid [1].

The original microgrid has 21 single phase transformers to supply just the residential sector and each commercial building has its own 3-phase step down transformer. For MATLAB Simulink representation, RLC load components connected in series and parallel are used to simulate the residential and commercial loads. The nominal voltage is 120V for the residential loads and 240V for the commercial loads [1]. Related data and diagrams for the original microgrid are shown in figures 1 through 10, and tables 1 through 4.

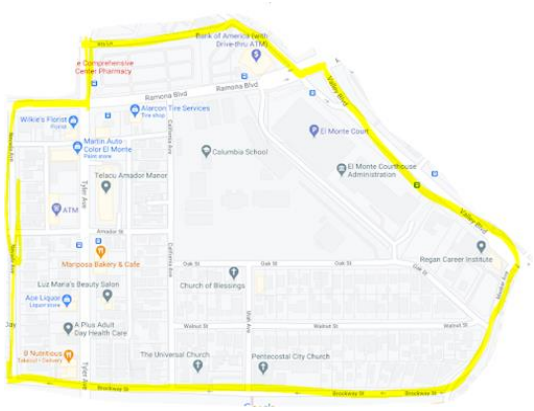

Fig. 1 Chosen area in El Monte city, California. The yellow line marks the area boundary [1]

Fig. 2 Air view of chosen area in El Monte city, California, showing the different grid lines. The red line is the gridline of Columbia, the green line is of Enloe, the yellow line is of Daroca. The gray line is also Daroca but is a single-phase line [1]

2.2 Battery parameters [1]

The microgrid load is the main factor that influences the selection of the battery system in addition to the cost, size, and safety factors. The selected battery is Samsung 30Q-18650 that is cost-efficient and easier to configure thanks to the cylindrical shape. The battery is used before sunrise and after sunset to supply the microgrid load. The shortest day of sunlight in Southern California is 9 hours and 55 minutes which means that the battery system needs to provide power for up to 14 hours on average per day. It was calculated that the energy required from the battery is 11,443.15kWh. Thus, connecting multiple

battery cells in series and parallel would sufficiently provide that power. The chosen battery ratings are 600 VDC, 25,500 Ah or 13.296 MWh. The battery estimated cost is 7,750,122 U.S. dollars. For brevity, readers are requested to refer to [1] where the battery parameters are described in details.

2.3 Solar PV system parameters

The solar PV system [1] is designed to supply all the energy demand of the microgrid. The daily average energy consumed by the load is used to find the size of the system. Because there are power losses in the distribution lines and inverter, the daily average energy consumed was increased by 10% to account for the losses. The model chosen is the Trina 400W Solar Panels 144 ½ Cell Multi-BB Mono TSM-400-DE15H(II). The average energy demand that accounts for losses is divided by the peak-sun hours which then converts the output needed into Watts. We multiply this value by the efficiency of the solar panels (19.7%, Table 2) to obtain the size for the PV system. This yields a DC solar PV system size of 4517.45 kW, as shown in Table 3.

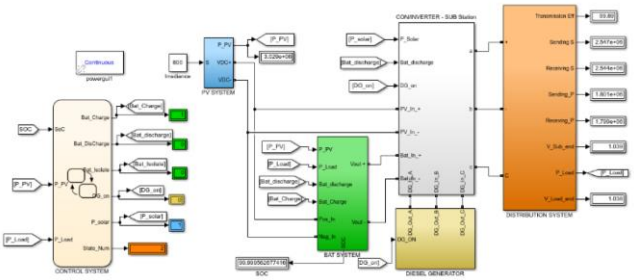

Fig. 3 Simulink diagram of original microgrid [1]

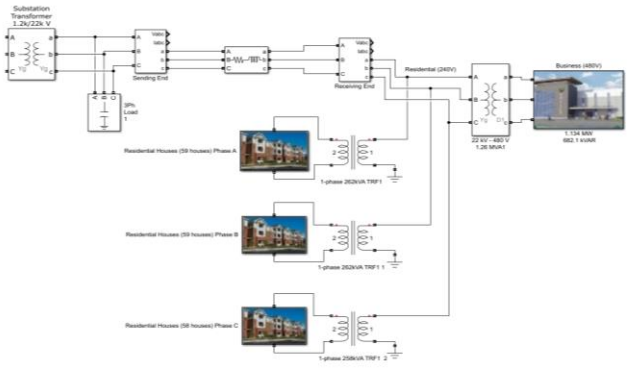

Fig. 4 Simulink diagram of original microgrid distribution section [1]

Table 1 Average energy and power consumption [1]

Parameter	Value
Annual Energy (kWh)	6,887,500
Average Energy Per Month (kWh)	573,958.33
Average Energy Per Day (kWh)	18,869.86
Average Real Power Per Day (kW)	786.24

Table 2 Solar panel characteristics [1]

Max Power Point Voltage (Vmpp) – (V)	47.40
Max Power Point Current (Impp) – (A)	9.74
Maximum Power Point (Pmax) – (kW)	0.46
Efficiency (%)	19.70

Table 3 Power and energy production of solar system [1]

Parameter	Value
Annual Energy Production (kWh)	39,572,862
Average Energy Production Per Month (kWh)	3,252,564
Average Energy Production Per Day (kWh)	108,418.8
Average Power Production (kW)	4517.45

Table 4 Battery cell characteristics [1]

Samsung 30Q-18650 Cell Characteristics	
Max Discharge Current	20A
Max Continuous Discharge Current	15A
Nominal Voltage (Vbat)	3.6V
Cutoff Voltage	2.7V
Capacity (at 10A Discharge)	3 Ah
Nominal Energy, (C,ideal = 3.6V * 3Ah)	10.8Wh
Capacity of a Cell with 70% and Depth of Discharge (DOD), C, DOD = 10.8Wh * 0.7	7.56 Wh
Capacity of a Cell with 95% Discharge Health (C) C = 7.56Wh * 0.95	7Wh

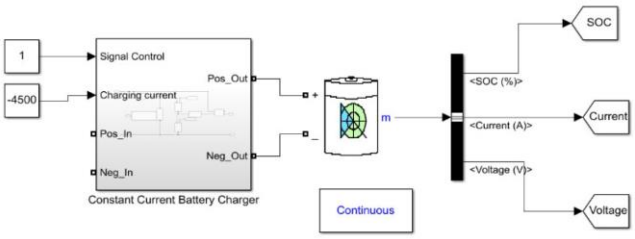

Fig. 5 Simulink-based battery system [1]

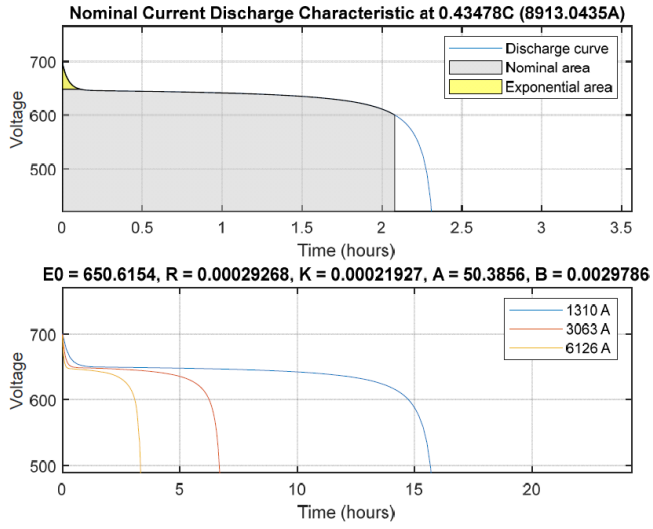

Fig. 6 Discharging characteristics of battery system [1]

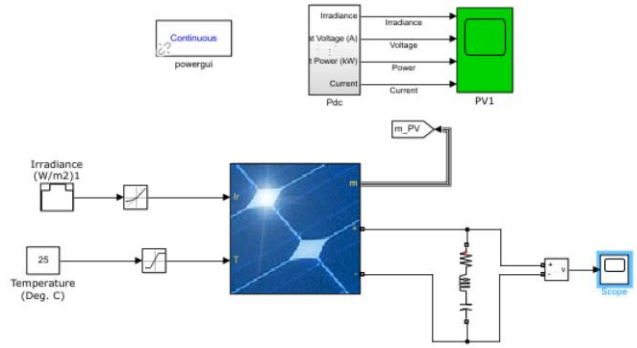

Fig. 7 Simulink-based PV system where temperature is at the standard testing condition of 25°C [1]

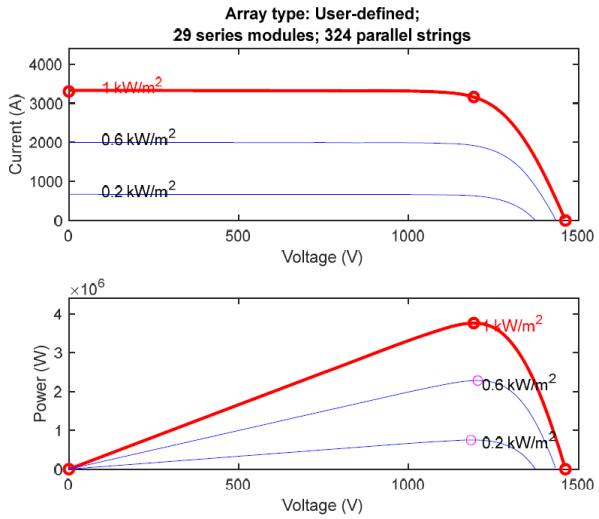

Fig. 8 Current, power, and voltage generated by the solar PV system in total for three different irradiance values. This applies to both the original and modularized systems [1]

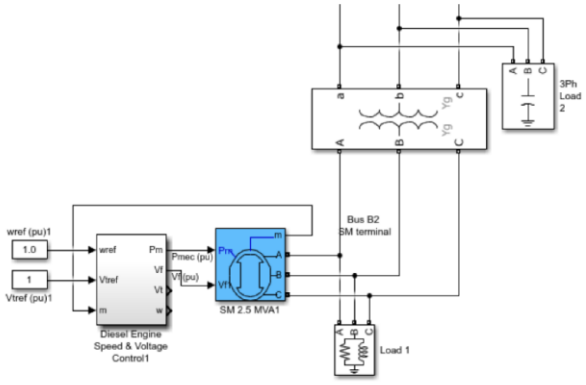

Fig. 9 Simulink-based diesel generator [1]

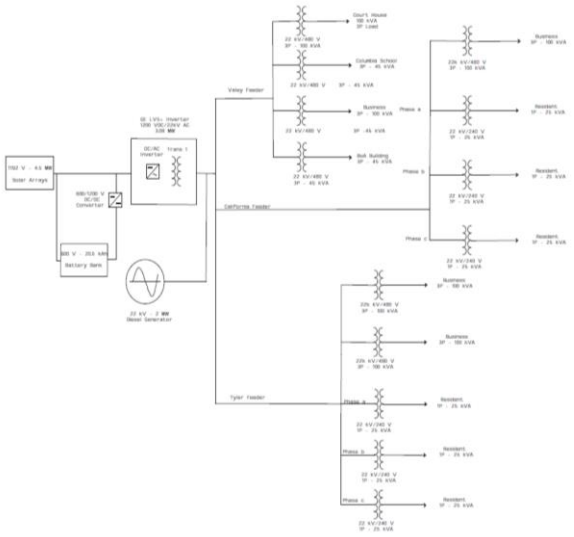

Fig. 10 Distribution layout for original microgrid [1]

2.4 Diesel generator parameters

The diesel generator (DG) is used to support the microgrid peak load conditions during any day and under normal conditions, such as cloudy days or other emergency situations. It is estimated that the generator should produce up to 2000kW. The model chosen for the diesel generator is the CAT 3516C 2000kW 480VAC Diesel Generator. There are approximately 282 sunny days and 83 cloudy days per year in El Monte. On sunny days, the diesel generator is used for around 3 hours to support the peak load at 92% of its rating. On cloudy days, the generator is used for around 13 hours per day at 50% of its rating. The generator's estimated price is 435,000 U.S. dollars. The total cost of fuel to operate the generator is estimated to be 738,423 U.S. dollars per year [1]

2.5 Original simulation and control logic [1]

The control system was implemented and tested using Simulink Stateflow which allows simulation of decision logic. In state flow there can be many different states, where the transition between states is based on a condition and variables, and the current state depends on the previous state. There is an entry and exit action that comes with every state. When a condition enters a state the entry actions are completed, once complete then the transitions actions are triggered. Once confirmed to move to another state the activities in the exit actions are completed. The states are determined based on what are the inputs for the system. The inputs for this system are PV Load, Battery's state of charge, and load demand from Simulink.

There are five different states representing five different scenarios for the original microgrid operation, with each scenario being a real-world event that is expected to happen.

State 1 is when the battery is the only source supplying the load and the solar PV and the DG are off. The simulation showed that the peak load power demand is 1.8MW and the battery alone can supply 12MW which is enough to supply the load.

State 2 is looking to use only the solar PV to meet the demand of the load and charge the battery. The irradiance at the time of peak load which is during the middle of the day is 1000W/m^2. The simulation shows that the output of the PV system is 3.7MW and the power demand is 1.8MW which is more than enough power for the load.

State 3 the scenario looked at is having the solar PV system supply the load and the battery is fully charged and disconnected from the system. This would be occurring at 4pm where the irradiance is around 600W/m^2. At this time the DG is off and the solar PV system produces 2.1MW which exceeds the power demand of the load at 1.9MW.

State 4 is when the load is exceeding the PV system output, the battery is charging, and the diesel generator must supply the load. In this scenario the irradiance is low and the battery is less than 20% charged so the diesel generator is supplying the load. This scenario can occur during the early morning hours during the winter. The diesel generator would succeed and supply the load with a voltage of 1.006 per unit.

Lastly, State 5 looks at when the diesel generator supplies the load when there is no power to be supplied by the PV system and the battery is less than 20% charge. This situation would be on cloudy days, night, or even emergencies. The simulation shows that the diesel generator can supply the load of 1.9MW with a voltage of 0.9868 per unit.

3. Improvement of original microgrid: supply-demand balancing using enhanced control logic, dummy load, and solar system modularization

3.1 Verification of original microgrid values

Before attempting to improve the original control logic, we verify the performance of the PV system. We were initially skeptical that the PV system was not producing the power and load demand essential in operating the generator.

$$Pmp_{module} = V_{mp} * I_{mp} \quad (1)$$

$$Pmp_{total} = Pmp_{module} * Module\ per\ String * Parallel\ String \quad (2)$$

$$\#\ of\ Modules * V_{mp} = Load \quad (3)$$

Using the equations listed above from [25] we were able to verify that the PV system was producing the correct values for our Power and Load demand.

3.2 Consideration of static var compensator

We considered a static var compensator (SVC) for controlling the microgrid overvoltage and undervoltage conditions. After analyzing the line impedance with various conductors on the microgrid for a line length of 20 miles, it was determined that conductors specifically rated for 22kV is more than sufficient in minimizing line losses and maintaining a required ±5% tolerance of the nominal voltage at the load, as recommended by power utility PG&E [26].

For analyzing the various conductors, their reactance and resistance of a 20-mile line are calculated using data for BareNRG™ ACSR aluminum conductor from CME [27]. Power distribution efficiency and receiving voltage were obtained by simulation of the original microgrid using the calculated impedance values.

With modularized solar PV system and a dummy loading aiding in overvoltage mitigation and the discovery that line power loss is not a key concern in our system, we have decided not to implement the SVC in our enhanced microgrid.

3.3 Control logic improvement

Although the original microgrid is detailed and thorough, there are rooms for improvement. One of the most notable issues is that there was no plan (and hence no control logic) to deal with excess power from the solar panels if the supply was greater than the demand. Without a proper solution the situation could lead to overvoltage conditions that damage the microgrid equipment.

In order to handle the excess power generated by the solar panels, we have revised the original control logic to make a new one, which is shown in Fig. 12 and
Fig 14. At the same time, we modularize the solar PV system by dividing it into modules that can be turned off to adjust the system output. A dummy load is also incorporated. Details are in sections 3.4 and 3.5.

Comparing with the original control logic (shown in Fig. 11 and Fig. 13), our enhanced control logic adds new states which link to the original State 3. Specifically, these new states (State 6 and a State 7) are attached to the original State 3. Thus, the states serving the purpose of overvoltage mitigation are State 3 (Battery Isolation), State 6 (Dummy Load Activated), and State 7 (Solar Modularization).

When being in battery isolation mode (i.e. the battery is not charging), if the PV system produces more than 1% of the load demand (1.01*Peak Load), then the control logic will enter State 6 and activate the dummy load to store the excess power. However, if the PV system produces less than 1.01*Peak Load, the control logic will stay in battery isolation mode.

When in State 6, if the PV system produces more than 1.01*(Peak Load + Dummy Load), then the logic will move into solar modularization mode (i.e. the solar PV output is regulated by turning off its modules). If the PV system produces less than 1.01*(Peak Load + Dummy Load), then the solar modularization is not activated. State 7 is broken down into multiple states labeled from State 7-12, to modularize the PV system and turn off solar modules

in decrements of 10% of its total power capacity. This logic will be explained further in following sections.

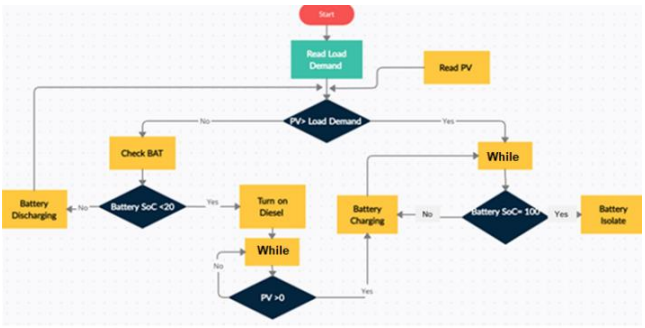

Fig. 11 Original microgrid control system logic [1]

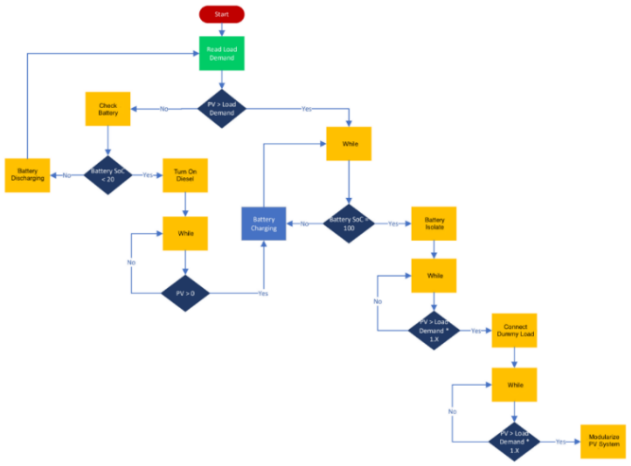

Fig. 12 New control logic for handling excess power that the solar PV system may produce

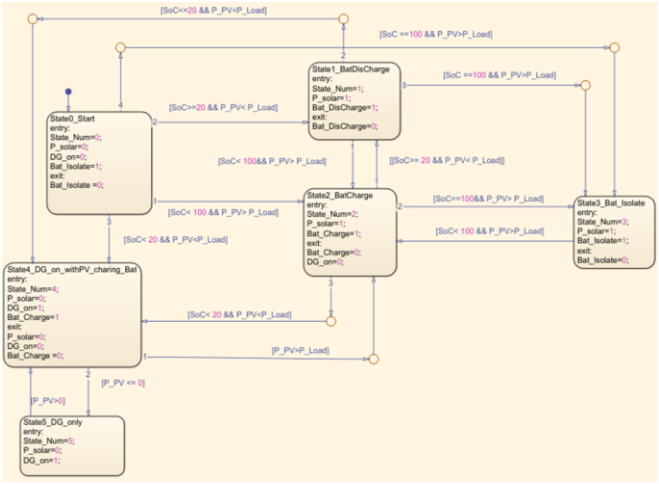

Fig. 13 Stateflow of control logic of original microgrid [1]

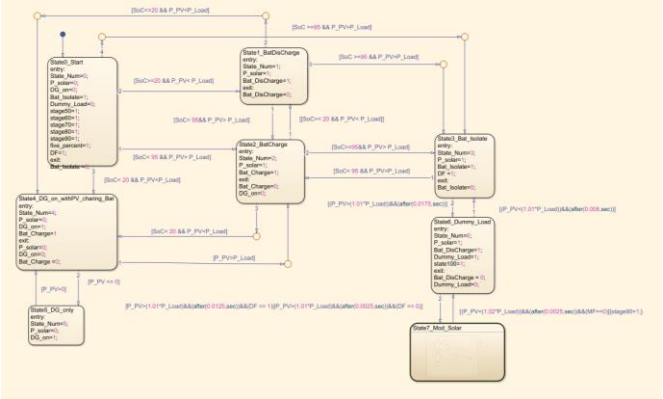

Fig. 14 New control logic stateflow with dummy load and modularized solar PV system

Table 5 Calculation of dummy load size

	Units	June	July	August
Solar Radiance	kWh/m^2/day	7.17	7.62	7.64
Avg Irradiance	W/m^2	896.25	952.5	955
PV_Peak	MW	3.39	3.596	3.605
Peak_Demand [1]	MW	1.8379	1.736	1.6075
Peak PV minus Peak Demand	**MW**	**1.5521**	**1.86**	**1.9975**
Dummy Load	**MW**	**0.54096**		

3.4 Dummy load implementation

The original design for the microgrid did not account for a scenario in which the battery was 100% charged and the solar power output was higher than the power demand. This excess power generation is harmful to grids as it can cause overvoltage conditions. In order to solve this issue a dummy load was implemented in the enhanced microgrid.

The dummy load is, in theory, supposed to use up the excess power generated in order to maintain supply-load balance. Since the original microgrid has a significant residential area, it was concluded that a water heating dummy load was the most useful as it can provide hot water to the residential areas.

The dummy load is placed in close proximity to the residential areas where the hot water would be used. The size of the dummy load is estimated to be 500kW, based on Table 5 data.

As shown by Table 5, the daily solar irradiance was found for the months of June, July, and August using the National Renewable Energy Laboratory (NREL) PV Watts calculator [28]. These months were chosen because that is the time frame in which Earth receives its highest solar radiance and thus PV systems produce their maximum power. Using the estimated solar radiance per day, the average irradiance for each individual month was calculated.

$$Average\ Irradiance = \frac{Solar\ Radiance}{8hr/day} \quad (4)$$

This value of average irradiance was then plugged into the Simulink simulation in order to produce the PV power output. The simulation results are in the row titled as PV_Peak, which means that the simulation PV system produced that amount of power for the given average irradiance. Then, the difference between the power generated by the PV system and the peak load demand for each corresponding month is found. The difference in power for each month was 1.5521MW(June), 1.86MW (July), and 1.997MW (August). The dummy load is supposed to take around 30% of the difference.

$$Dummy\ Load = Avg\ of\ 30\%(Peak\ PV - Peak\ Demand) \quad (5)$$

When averaging all 3 values out, the calculations show that the dummy load should be consuming about 540kW. The value for the dummy load size is rounded from 540kW to 500kW in order to make other calculations and simulations easier.

The real life implementation of the water heater dummy load uses a water heater manufactured by AO Smith Electric Water Heaters [29]. The water heater chosen is the model DHE-800A which utilizes 240V/480V and can consume a maximum power of 720kW. Even though this water heater can take up to 720kW of power, it is assumed that it is only going to consume 500kW. With the 500kW power consumption, the water heater is able to run without being pushed to its maximum limit and still performs its intended job. Not running the water heater at its maximum power capacity allows for safe and long-lasting use of this electrical equipment.

The dummy load implementation on Simulink used an RLC load block. The specifications for this load block assumed that it was receiving 480V and the power consumption for the load was set to 500kW. When the simulation was run, the measured power consumption for the load block was 508kW which is close to the theoretical rating of 500kW. The water heater chosen for the real-life implementation is able to withstand this small deviation in power.

3.5 Solar system modularization

The solar PV system is divided into modules to decrease the power output in steps. The solar modularization control logic and part of the modularized solar system are shown in Fig. and Fig. 18. The logic is implemented in sub-states which are consolidated in State 7 of the microgrid main control logic (Fig. 14). The ideation and calculation behind this logic is shown in Table 6.

Referring to Table 6, the Peak Load Demand parameter is referenced from the original microgrid [1]. The Dummy Demand parameter was calculated in the previous section, with a value of 500kW. Total Demand is calculated as:

$$Total\ Demand = Peak\ Load\ demand + Dummy\ Demand \quad (6)$$

Parameter named "% PV Kept Constant" refers to what percent of the solar output power we believe is safe to always keep on, as it would never result in overpowering the monthly load demand. It refers to what percent of the solar output power we believe is safe to always keep on, as it would never result in overpowering the monthly load demand. It is calculated as

$$\%\ PV\ Kept\ Constant = Total\ Demand / Max\ PV\ Output \quad (7)$$

where Max PV Output is about 3.7MW as tested and verified in our system from our chosen solar panels. It follows that

$$\%\ PV\ to\ Modularize = 100\% - \%PV\ Kept\ Constant \quad (8)$$

From Table 6, at most 44% of the solar system total capacity needs to be modularized for load following (balancing). To have more flexibility to regulate the solar system output, we decided to modularize 50% of the solar panels. The modularized panels are subdivided by decrements of 10% and 5%.

If implemented in an actual microgrid, the hardware for the solar modularization is likely to involve relay switching matrices, similar to those involved in the literature discussing dynamic array reconfigurations [12-14].

3.6 Conditions for control logic proper operation

This section explains important conditions that we developed to ensure that both the main control logic and the solar modularization logic work properly. Recall that the enhanced main control logic is shown in figures 12 and 14 while the solar modularization logic is shown in Fig. 17.

Referring to Fig. 17, the Sub-States 7-12 are consolidated within State 7 of the main control logic, representing the modules turning off in decrements of 10% for each state. Intermediate states (State 7.5, 8.5, and 9.5) represent the toggling of the 5% module.

In order to move forward through the states, the condition must be met that the PV power production was greater than the safe limits of the load power demand (arbitrarily chosen to be above 1%). For example, in order to transition from State 3 to State 6 if the load demand is 1.8MW, then PV would have to produce at least 1.818MW. This would in-turn activate the dummy load.

On the other hand, in order to transition from State 6 to State 7, the dummy demand of 500kW is now added onto the 1.8MW, resulting in a total demand of 2.3MW. And so now, the power generated by the PV system would have to be at least 2.323MW to begin switching off solar modules, starting with 10% being turned off.

For the solar module States 7-12, the respective percentage of solar already turned off needed to be considered prior to transitioning. For example, the condition to move forward from State 8 to State 9 requires: "(P_PV - 0.1*P_PV) > (1.01*P_Load)". Thus, in order to switch off the 20% of solar modules, it must first be confirmed that the power generated would still be greater than the load demand even after switching off the first 10%. Each consecutive state transition continues to subtract another 10% from the solar system power output.

Fig. 15 Electric water heater model DHE-800A used as a dummy load

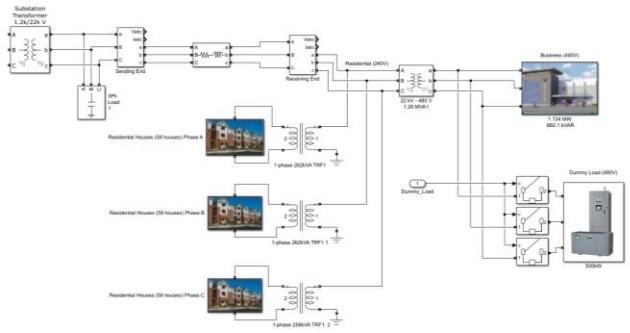

Fig. 16 Simulink-based distribution system including dummy load

Table 6 Calculation of solar system power for modularization

Parameter	June	July	August
Peak Load Demand (MW)	1.8379	1.736	1.6075
Dummy Load (MW)	0.5	0.5	0.5
Total Demand (MW)	2.3379	2.236	2.1075
% PV Kept Constant	62.1617	59.4523	**56.0356**
% PV To Modularize	37.8383	40.5477	**43.9644**

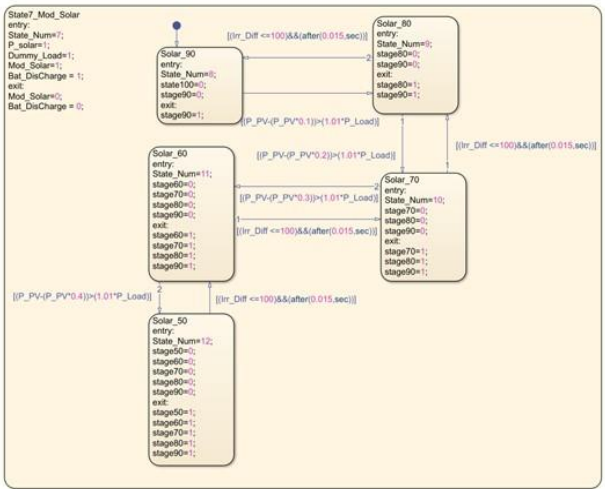

Fig. 17 Stateflow chart for modular solar Sub-States 8-12 consolidated within State 7

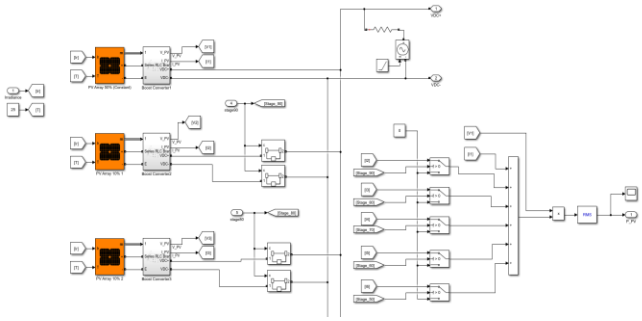

Fig. 18 A portion of the modularized Simulink-based solar system

For the solar module States 7-12, the respective percentage of solar already turned off needed to be considered prior to transitioning. For example, the condition to move forward from State 8 to State 9 requires: "(P_PV - 0.1*P_PV) > (1.01*P_Load)". Thus, in order to switch off the 20% of solar modules, it must first be confirmed that the power generated would still be greater than the load demand even after switching off the first 10%. Each consecutive state transition continues to subtract another 10% from the power output.

After establishing a logic process for progressively turning off our solar modules, the conditions for turning the solar array back on completely needed to be set to allow for the microgrid to flow seamlessly in and out of modular scenarios. During testing it was discovered that if the same conditions that led to the modules turning off were used to return back to a previous state, the control logic for the microgrid would get caught between going back and forth between states while measurements were stabilizing. To avoid this, a different set of conditions was desired.

Currently on the system, logic bringing our microgrid back to utilizing 100% of the solar system is determined by checking that PV power is greater than 1.X load demand. In addition, a time buffer is also in place to prevent alternating back and forth between states.

For modules where larger portions of our PV array are turned off, a larger multiplier is used to calculate load demand to ensure that the system can react within an appropriate amount of time to turn portions of the PV array back on without ever having PV power fall below demand. However, even though PV power should not fall below demand, nor should it be excessively above demand as to avoid overvoltage issues. With our 10% decrements this left a buffer of supplying about 360 kW in excess in a worst-case scenario. To also limit this, the 5% PV array is used to not only ease transitions between 10% decrements but to also halve our potential worst-case scenario of excess power supplied to 180 kW. At any point though, if load demand exceeds power by any given multiplier depending on the current stage, the PV system will turn back on in portions of 5% within 0.25 milliseconds.

In addition to our increment and decrement conditions that allow for the PV array to seamlessly transition through varying impedance scenarios, a key feature that ensured a stable and level PV power output over load demands was the inclusion of an active and idle state that continuously paused our system every 0.5 ms for 0.5 ms. This smoothed scenarios in which frequent oscillations occurred between 3 different states due to measurements falling too close to the given buffer conditions causing premature increments or decrements before the system could stabilize. The continual active and idle stage utilized a hub state upon return to the active state to be able to connect back to every modularized

PV scenario and only brought the system back to the state at which it left off. This did not prevent oscillations between states but allowed the PV system enough time to see the steady state result of turning on and off specific PV modules allowing for more accurate measurements, in turn ensuring the system was operating in the correct state.

3.7 Simulation results for testing dummy load, modularized solar system, and control system

Base Scenario: No load or power balancing. The PV system has already been modularized but switching control logic is not activated.

Results: Figure 19 illustrates that the modularized PV system is capable of producing the same amount of power output as the original microgrid's single PV array (3.7MW steady state P_PV). Thus, in testing the various scenarios, we know that the outputs are not hindered by modularization, and are accurate based on irradiance input and the percentage of modules kept on.

Scenario 1: First stage of overvoltage mitigation, battery is isolated when it is full and PV produces slightly more power than the load.

Results: For this scenario, the irradiance range is between 474 W/m2 and 482 W/m2. The system enters State 3, leaving the PV at 100% operation and logically isolating the battery at time t=0.016s (Fig. 20). At this range, the PV output between 1.776MW and 1.801MW in steady state. However, around t=0.12s, the PV peaks just above 1.8MW, which is the power threshold required by the control logic. Thus, it is shown that State 3 of the logic is achieved when the PV system produces at least 1% more than the demand.

Scenario 2: Second stage of overvoltage mitigation, the dummy load is activated when battery is being full and PV produces over 1% more power than the load. Since the load demand including the dummy load may increase above what the PV system can provide under lower irradiance scenarios, the battery is also discharged to compensate for the necessary power that the solar system alone cannot provide.

Results: Scenario 2 ranges from 483 W/m2 to 616 W/m2 irradiance. The peak PV power output at 483 W/m2 irradiance is about 1.836MW at t = 0.118s. Then the PV power output at steady state averages around 1.805MW. Scenario 2 is exemplified in Fig. 21 which is ran at 500 W/m2 irradiance. At this point, the load and the dummy load of 500kW are both active, and so the new total load demand combining them is 2.3MW. Since the PV output is now underproducing, the switch to discharge the battery was activated to supply the extra power needed for the load. In this scenario, when the irradiance is 616 W/m2, the peak power output of the PV is 2.340MW at t=0.097s, which is almost the same as the load (2.3MW load). Again, the switch to discharge the battery is successfully set as active to supply the extra needed power for the main load and dummy load.

Scenario 3: Third stage of overvoltage mitigation, PV system output is regulated by switching one of its modules off when the PV system produces over 1% more power than the load at a constant irradiance of 720 W/m2. Since the modules switch off in increments of 5% at minimum, there are some irradiance scenarios in which the PV system has turned off too much power and slightly underproduces for the load. For example, if the load requires an extra 1% of power, the solar system can only either overprovide by 4% or underprovide by 4%. Thus, when the control logic chooses to underprovide, the battery is discharged in order to compensate for the excess solar modules switched off.

Results: Scenario 3 forced the simulation to enter State 7 by checking if the power produced by the solar modules is greater than 101% of the power demand caused by the load. Once the simulation was in State 7, a signal was sent to the circuit breaker controlling one solar module which produces 10% of the total power generated. The signal turned off the module and limited the solar module output to 90% of its maximum capacity based on the given irradiance. Scenario 3 is exemplified in Fig. 22, which also discharges the battery to compensate for irradiance scenarios where solar power is unable to fully provide for the 2.3MW load demand.

Scenario 4: Solar modularization involving variable irradiance. In order to achieve the different states, the following irradiance values were used: [470, 610, 720, 825, 940, and 1000] W/m2. Battery is discharged in order to compensate for the solar modules switched off.

Results: Figure 23 gives the system measurements for this scenario. As irradiance in the system is gradually increased, the power supplied by our PV system increases in tandem. Once the power supplied increases to a level greater than 370kW in comparison to our load demand, modular solar becomes active and turns off 10% of our solar system at a time. To smooth the transition between the 10% modules, the 5% module toggles on and off as well. The power supply and the load demand are close as shown in Fig. 24.

While there is a frequent oscillation between state numbers, we can see there is a maximum difference of 156.6kW and that the power difference is maintained well below 10% (370kW). The PV output is also stabilized such that there is not much change in power when switching between states. This effectively shows the microgrid's capability to handle varying irradiance levels and is much improved compared to our previous iterations of the control logic.

Scenario 5: PV system produces a constant power far more than the load and battery can handle, 40% of the solar system is switched off. Battery is discharged in order to compensate for the solar modules switched off.

Results: Ultimately, results follow much like Scenario 4 except instead of step irradiance, the maximum irradiance of 1000 W/m2 is used. While our solar system can turn off up to 50% of its capacity, this scenario shows that only a maximum of 40% of our solar system is to turn off at any given point in time since our expected loading of 2.2 MW cannot be met if only 50% of the system is left on as it would only be able to supply 1.85 MW. Thus, there is an extra 10% buffer in case if extensive overvoltage is somehow achieved beyond expectation. With this highest power supplied scenario in mind this shows that modular solar and dummy loading in tandem should be able to accommodate for any scenario in which generation is greater than our given load demand, including the worst-case scenario in which the load demand is significantly less than the solar power produced.

Scenario 6: Variable irradiance is applied decrementally instead of incrementally to verify that the control logic is able to turn modules back on as well. Scenario 4's irradiance values are considered in a reverse order: [1000, 940, 825, 720, 610, and 470] W/m2.

Results: Figure 25 reveals successful results which are very similar to Scenario 4. Again, there are very frequent oscillations between State numbers. Even so, Fig. 26 again shows minimal ripple and a maximum difference between PV Power and load demand of up to 174.3kW, which is again well below the 10% tolerance. This is a great improvement compared to previous iterations which resulted in PV power exhibiting volatile behavior returning to many previous states during irradiance changes.

Overall, the results from the tested scenarios show that the control system can handle both increasing and decreasing changes in irradiance.

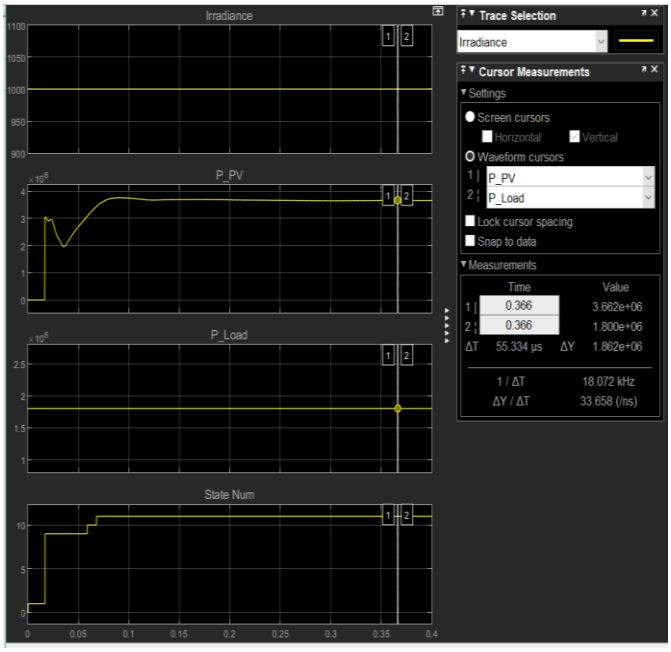

Fig. 19 Simulation results when load and power balancing are disabled for the Base Scenario

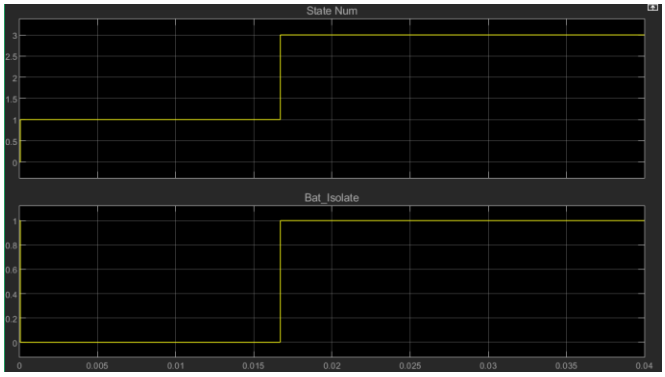

Fig. 20 Scenario 1 simulation results indicating that for State 3 of the control logic, the battery is logically isolated at t = 16ms

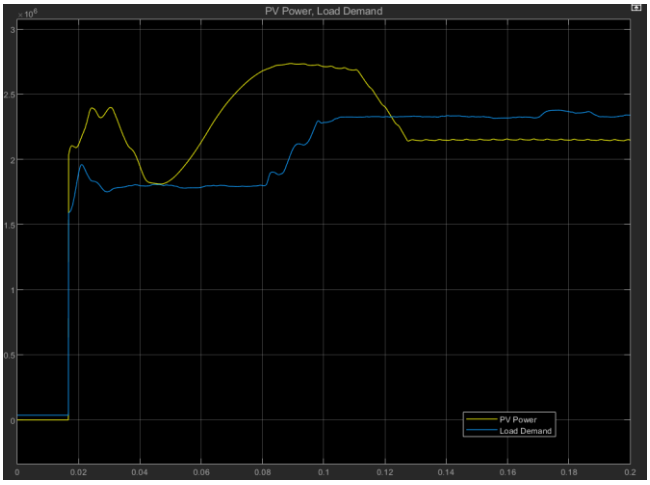

Fig. 22 PV Power versus Load Demand for Scenario 3 at 720W/m2 irradiance. Solar modules are switched off at t = 0.11s, mitigating overvoltage. Like Scenario 2, any power not covered by the solar system is compensated by discharging the battery

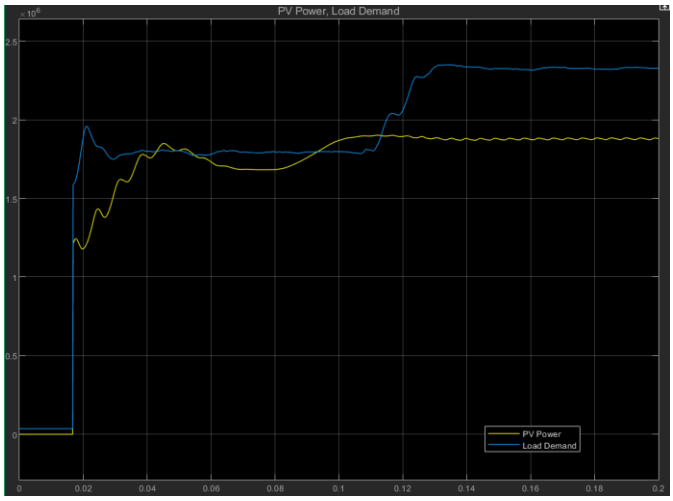

Fig. 21 PV Power vs Load Demand for Scenario 2 at 500W/m2 irradiance. PV surpasses 10% load demand at t = 92ms. Dummy load activates at t = 110ms. Total demand becomes 2.3MW. Any power not covered by the solar system is compensated by discharging the battery.

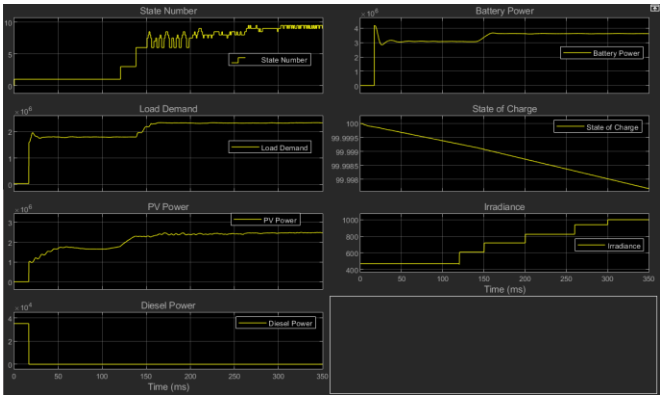

Fig. 23 System measurements for Scenario 4

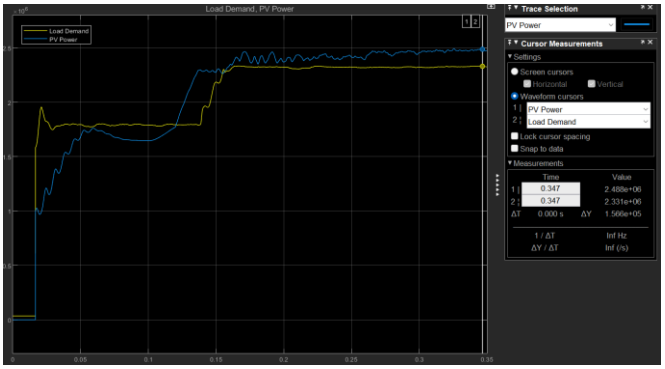

Fig. 24 PV Power versus Load for Scenario 4

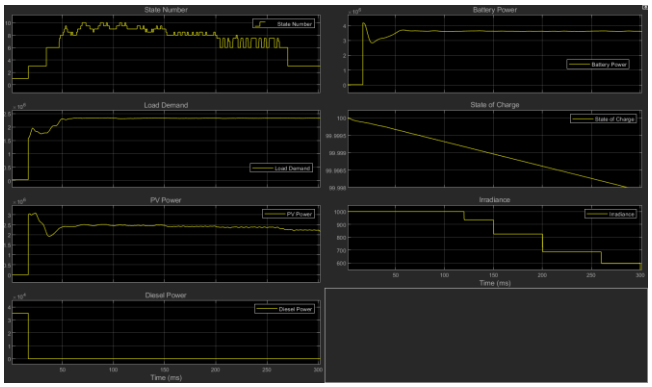

Fig. 25 System measurements for Scenario 6

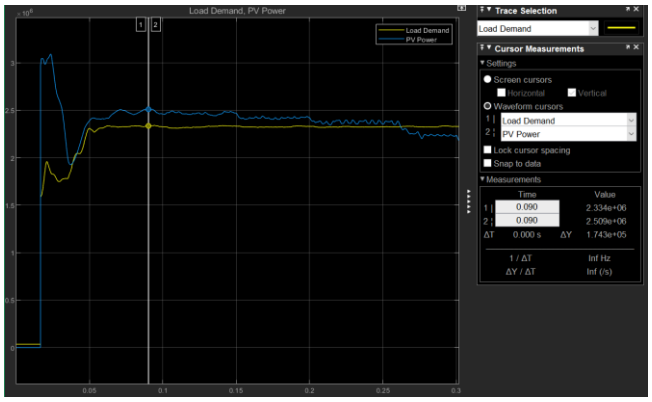

Fig. 26 PV Power versus Load Demand for Scenario 6

4. Development and implementation of a relay system for fault interruption

4.1 Relay system overview

The original microgrid design did not have a protection system in place to address any issues arising from external factors that may down a power line, such as fallen trees or severe weather conditions. To resolve this vulnerability, an overcurrent relay system was designed to detect and isolate the fault quickly to minimize the damages to electrical equipment, the environment, and ensure safety for human beings. Circuit breakers and a control system using stateflow logic are used to resemble automatic reclosers. Since most short-circuit faults are temporary due to trees, small animals, or weather conditions, a recloser helps cut the power to the lines and gives the system a chance to return to normal before turning off the power permanently. Distribution circuits typically have these relay systems in place to ensure a more robust system that can provide electricity quickly and automatically to customers with minimal downtime. Recovering from an interruption is paramount for critical infrastructure like our microgrid and this is accomplished by the protective relay system.

4.2 Relay stateflow logic

The scheme used for the relay stateflow logic in Fig. 27 is two-fast and two-delayed [30, 31]. The logic will remain in state zero until a fault current that is higher than the reference current is detected.

The relay stateflow logic is broken down into a simple flowchart in Fig. 28. Once a short circuit fault occurs on a power line, the first fast trip will open the circuit breakers at the receiving and sending end of the distribution line after the system sees the faulty current for 0.05 seconds. The circuit breakers will remain open for 0.5 seconds and then close again to allow the system to check the fault current again.

If the fault has already cleared on its own, the stateflow will return back to state zero and remain closed, but if the fault current is still present, the circuit breakers will open once more after 0.05 seconds for the second fast tripping of 0.5 seconds.

If the fault is still not cleared, the circuit breakers will repeat the same tripping and reclosing method but will now wait 5 seconds before reclosing and reading the fault current. Again, if the fault has cleared, the stateflow will return to state zero. If not, the breakers will open after 5 seconds. This slow tripping will occur once more and if the fault is not cleared after this, the breakers stay open indefinitely.

4.3 Relay system testing results

In order to test the relay system before adding it to the microgrid, a smaller power system was created which is shown in Fig. 29. This includes a 3-phase source, two 3-phase loads, a 3-phase fault, and two 3-phase circuit breakers connected to both the source and the loads.

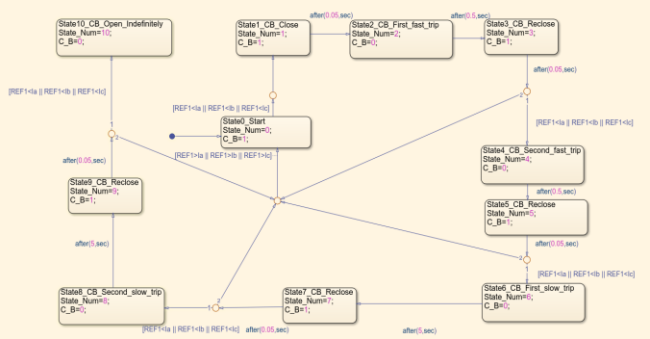

Fig. 27 Relay stateflow logic

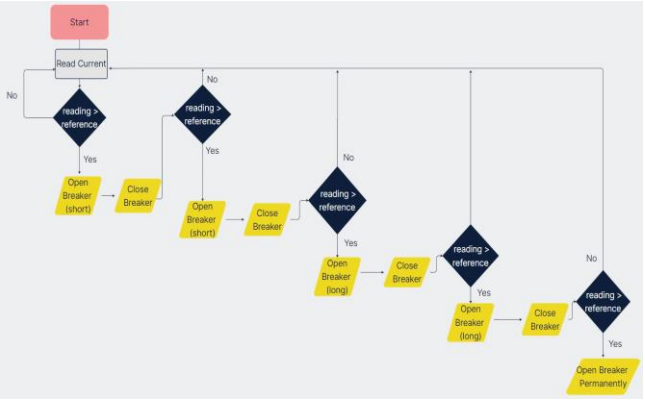

Fig. 28 Relay sequence flowchart

The stateflow in Fig. 27 is used for the control system to determine whether the circuit breakers are open or closed. The two types of faults on a power system include a transient or temporary fault and a permanent fault in which a field crew must be sent out to repair the damaged equipment. When initiating a fault in the small power system, the relay stateflow will circulate through the different states depending on when and if the fault clears on its own. Another point to note is that when the circuit breakers reclose, there is a minimal spike of current and a delay in reading the current is needed.

Scenario 1: A temporary single-line-to-ground (1LG) fault occurs on the system caused by a small animal or object on the distribution line.

Results: Figure 30 shows what the 3-phase current looks like for the system when a temporary 1LG fault occurs. In this case, the fault was cleared before the third trip. The first spike in the graph is when the fault initially occurs, and the relay system is delayed 0.05 seconds before opening the circuit breaker for the first time. The next two spikes that are separated by 0.5 seconds are considered the two fast operations in the logic scheme. The first delayed operation starts to occur with the circuit breakers opened for 5 seconds, but since the fault is cleared after this, the current returns to normal and the stateflow logic returns to State 0.

Scenario 2: A temporary 2-line-to-ground (2LG) fault occurs on the system caused by a lightning strike or a tree branch touching the lines.

Results: Figure 31 shows what the 3-phase current looks like for the system when a temporary 2LG fault occurs. In this scenario, the fault was cleared before the fourth trip. The first three pulses in Fig. 31 remain the same as the last scenario while the fourth pulse shows the first delayed operation completely. The system then opens the circuit breakers one more time for a second delayed operation of 5 seconds and since the fault has been cleared during this delay and the current returns to normal, the system sees the proper current when the circuit breakers open and the stateflow logic returns to State 0.

Scenario 3: A permanent 3-line-to-ground (3LG) fault occurs on the system caused by tree branches falling on the distribution lines.

Results: Figure 32 shows what the 3-phase current looks like for the system when a permanent 3LG fault occurs. For this case, the fault was never cleared and the relay system sees faulty current at all four trips of the two fast and two delayed schemes. The circuit breakers remain open when the system is still measuring fault current after the entire scheme of about 11.25 seconds occurs. The fault has not cleared in time and the circuit breakers will remain open until the fault is fixed manually.

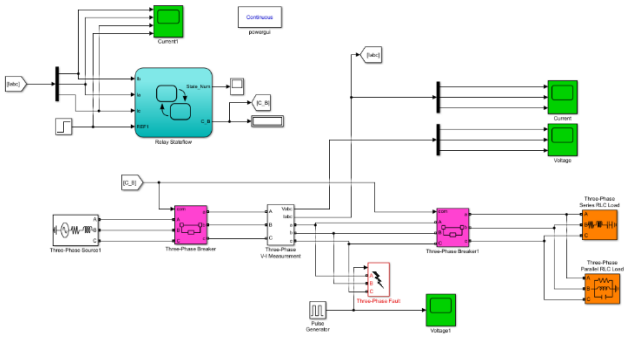

Fig. 29 Power system used to test the relay logic

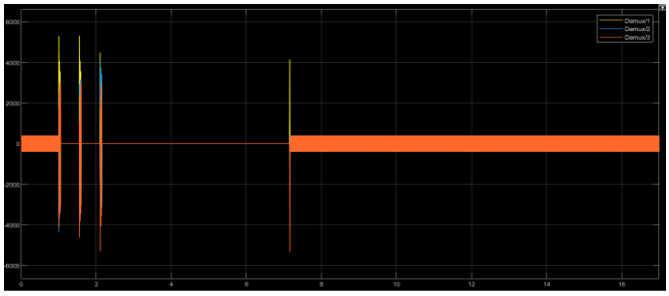

Fig. 30 Line current behavior for Scenario 1 where a temporary 1LG fault occurs and the relay system acts to clear the fault.

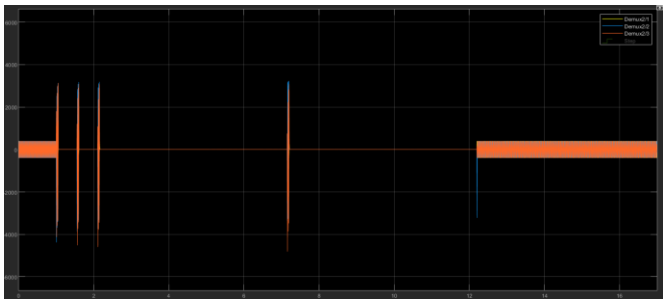

Fig. 31 Line current behavior for Scenario 2 where a temporary 2LG fault occurs and the relay system acts to clear the fault

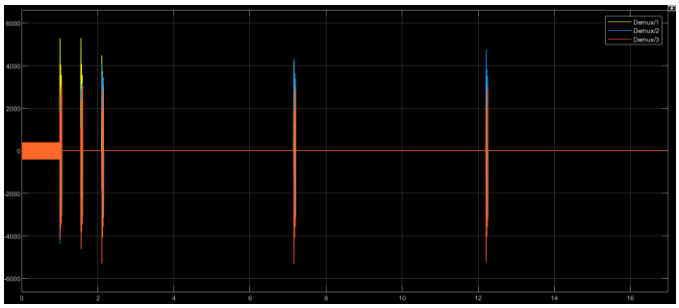

Fig. 32 Line current behavior for Scenario 3 where a permanent 3LG fault occurs and the relay system is unable to clear the fault

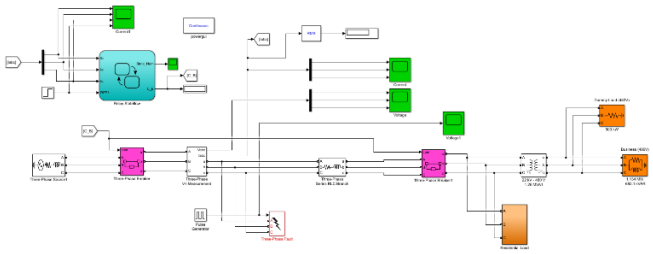

Fig. 33 Power system used to test the relay logic with the microgrid load

Table 7 Calculation of nominal currents

	Microgrid		Relay System	
	RMS Current w/Dummy [A,rms]	RMS Current w/out Dummy [A,rms]	RMS Current w/Dummy [A,rms]	RMS Current w/out Dummy [A,rms]
Peak Load	39.25	50.3	38.06	54.12
Average Load	38.77	30.8	37.91	23.39

4.4 Average and peak load data for use with relay system

To simulate how the relay system will react when being placed into the microgrid, we added the everyday load use of the Southern California El Monte region. Since the load value changes every day, the average and peak load of the El Monte region was used for simulation. For the relay system to work, a correct reference current must be chosen that will not trip the circuit breakers on a peak load day when the current is large but will still trip if there is a smaller faulty current. To determine this reference current, the nominal current at average and peak load were recorded along with the faulty current at different voltage sag percentages. After this, a reference current can be chosen that has a value between the highest nominal current and the lowest faulty current.

The average load value was determined in Table 1 with an average real power per day of 786.24 kW. According to the U.S. Energy Information

Administration, the average energy per month for an American household is 893 kWh, and through calculations, one household has an average real power per day of 1.24 kW [32]. The peak load value was determined earlier in the report to be 1837.9 kW. These values are used to create the load model from the microgrid shown in Fig. 33.

A dummy load of 500 kW is also added to the load model which matches the dummy load that was designed for our enhanced microgrid. Since this dummy load only turns on occasionally when the microgrid is producing too much power, simulations were done with and without the dummy load. With the system complete, the nominal current was measured and shown in Table 7. These nominal currents were also compared to the nominal currents in the microgrid to make sure the simulation was replicating the microgrid properly. Table 7 proves that the currents are similar enough to use for the relay system and the reference current must be higher than 55A for the system to work.

4.5 Voltage sag overview

According to IEEE definition, voltage sag is a decrease in voltage for a short period of time, often measured in cycles. The voltage sag magnitude can vary between the 10% and 90% of the nominal RMS voltage at 60 Hz [33]. Voltage sag is costly and must be considered in any power system as common electronics are sensitive to voltage deviations and may be at risk of potential damage. Voltage sags are a major power quality concern for most customers and electric utilities. The voltage reduction magnitude can be anywhere between 10% and 90% of the normal root mean square (RMS) voltage at 60 Hz as it can be caused by any unintentional surge of current either by large induction motors or faults such as those caused by falling tree branches. Furthermore, voltage sag magnitude percentage will vary to how close the fault location is to the customer.

To improve voltage sags, relays can be implemented in the power system to trip quicker for any faulty current detection. Other improvements such as installing arresters can also be used which in return help limit high magnitude current caused by lightning strikes. During a period of a voltage sag, customers may experience problems such as flickering or loss of power for certain home appliances. Therefore, a protection scheme must react fast for anytime the power quality decreases below an unacceptable value. Hence, improving voltage sags in a power system will reduce faults and minimize impact on customers.

To ensure the voltage sag issue is addressed by our overcurrent relay, a voltage sag test was conducted for peak and average load. This test verified that the circuit breakers would trip correctly when a voltage sag occurred. Additionally, this test helped to ensure the correct reference current value so that the relay would not activate under normal system conditions.

Table 8 Calculation of fault current for average load

Average Load			
Nominal Voltage: 22kV			
Sag to % Nominal	Voltage Level (kV)	Fault Resistance (Ron, ohm)	Fault Current (A rms)
90%	19.8	17.9	1076
80%	17.6	9.9	1695
70%	15.4	6.8	2141
60%	13.2	5.0	2486
50%	11	3.73	2766
40%	8.8	2.75	2992
30%	6.6	1.95	3170
20%	4.4	1.23	3312
10%	2.2	0.6	3414

Table 9 Calculation of fault current for peak load

Peak Load			
Nominal Voltage: 22 kV			
Sag to % Nominal	Voltage Level (kV)	Fault Resistance (Ron, ohm)	Fault current (A rms)
90%	19.8	17.6	1069
80%	17.6	9.7	1702
70%	15.4	6.8	2128
60%	13.2	4.95	2488
50%	11	3.7	2766
40%	8.8	2.75	2988
30%	6.6	1.93	3171

20%	4.4	1.24	3309
10%	2.2	0.6	3413

4.6 Voltage sag testing to determine reference current for relay system

Using the same power system but with the microgrid's load, we then looked at different fault impedance scenarios to see what caused voltage sags of varying percentages ranging from 10% to 90% of the nominal voltage. The voltage level of the sag percentage was achieved by means of trial and error by adjusting the fault resistance value to match the output voltage value. With each voltage sag percentage, the fault resistance and fault currents values were recorded. The voltage sag was recorded for two different loads, the average load and the peak load for a single phase only. The two loads were determined by city data online. Tables 8 and 9 show the data acquired during testing.

For both average load and peak load tests, when the voltage sag percentage decreased, the circuit breakers continued to trip and the fault current increased. After recording the fault current values and comparing them to the nominal current values, a reference current of 500A was determined for the control system. This reference current is higher than all normal currents and lower than all faulty currents, so a current at peak load will not trip the circuit breakers unless there is a fault. Additionally, the relay scheme has enough flexibility to operate under average load for a voltage sag of 10% below nominal rms voltage. Overall, the data from this test supports the reference current value of 500 A and should suffice for downtown El Monte since it would not experience any significant load growth due to limited space and its fixed service area.

5. System-wide simulation results

Figure 34 show the Simulink implementation of our enhanced main control system and Fig. 35 shows the entire enhanced microgrid. For evaluating our microgrid, we simulate different scenarios, where each scenario is a situation that may happen in a real world environment. For all normal operation scenarios (Scenario 1 through Scenario 5 below), voltage levels of both residential and commercial loads are maintained within a ±5% tolerance of their respective nominal values of 120V and 240V.

Scenario 1: Only the battery provides power to the load when solar irradiance is too low.

Results: The battery is set to a State of Charge of 80% in this scenario. The load is measured at a steady state of 1.54MW. Thus, since the PV system is only producing between 1.51MW at an irradiance of 400 W/m2, State 1 of the control logic is entered. As expected, only the battery is discharging to the load demand, while the PV system and diesel generator remain disconnected.

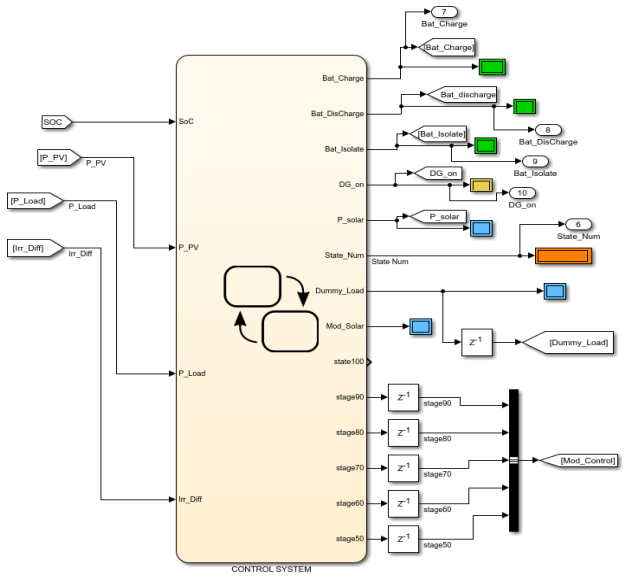

Fig. 34 Final Simulink-based enhanced main control system

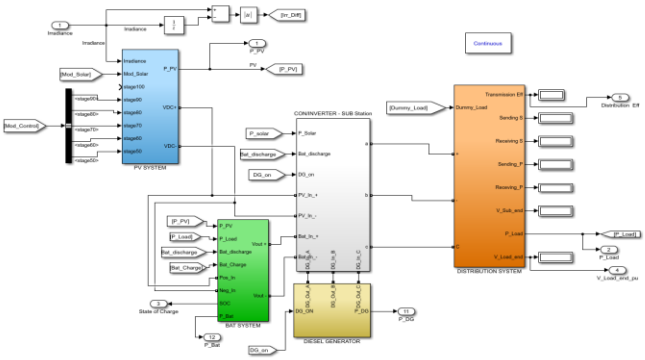

Fig. 35 Entire enhanced Simulink-based microgrid

Scenario 2: Irradiance is enough for the PV system to provide for the load. It also recharges the battery.

Results: The threshold for battery charging was changed from the original logic's 100% to 95%. Thus, when setting the battery's State of Charge to 80% and using a constant irradiance of 1000 W/m2, we find that the simulation enters State 2 of the control logic. However, there is some troubleshooting necessary for this state, as although the battery has entered charging mode through the PV system, the battery's State of Charge continues to deplete. This is unusual considering that the battery is successfully capable of recharging when the system is in State 4 or 5. In spite of the abnormal behavior, the solar power of 3.76MW with all modules turned on continues to provide for the 1.526MW load demand (assuming the battery is being recharged as well). The diesel generator also remains disconnected as expected.

Scenario 3: Overvoltage protection when the battery is close to fully charged and the solar system produces more power than the load and the battery can handle.

Results: The worst-case scenario is considered when the battery is at 100% State of Charge (SOC) and irradiance is at 1000 W/m2. At this time, the simulation consecutively enters State 3 (Battery Isolation), State 6 (Dummy Load Activation), all the way up to Sub-State 11 (40% of the PV system turned off). This shows that the control system functions properly. In measuring the residential and commercial voltage levels, it was found that prior to activating the dummy load and solar modularization, the voltages were up to 133V and 263V respectively, i.e. well beyond the +5% tolerance safety limits of 126V and 252V. However, once the overvoltage mitigation process was activated, the voltage levels dropped and stayed within permissible limits at 123V and 245V respectively.

Scenario 4: Diesel generator supplies power for the entire system while the load demand exceeds the power output of the PV system and the battery is discharged below safe levels.

Results: The safe discharging level chosen for the battery is 20%. Hence, when setting the battery's State of Charge to 15% while the irradiance is only 400 W/m2, it is found that neither the solar or battery system are able to provide for the load demand. However, the current re-integrated system does not yet work as intended. At the moment, the load demand drops to 0W when battery levels are below 20%.

The intention is that State 4 would be initially achieved and only the diesel generator is shown to provide the load while the PV and battery remain in charging mode. And when the irradiance is set to 0W/m2 (no sunlight), State 5 would be achieved. Further investigation and testing are required to fix this situation.

Scenario 5: Faulty conditions are split into three groups for testing, namely, (a) PV with SLG fault, (b) battery with 2LG fault, and (c) diesel with 3LG fault.

Results: System works properly the same way as shown in Section 4.

6. Troubleshooting and lessons learned

6.1 Troubleshooting

To troubleshoot the system unusual behavior in Scenario 4 of Section 5, each of the power sources was isolated along with the load to test which may have been the cause of the problem. In addition, further testing was done by swapping different components on the microgrid. Our main effort was swapping the current DC/AC converter with another of similar construction to observe if the interplay

between solar/battery and the converter is a cause. Here is a summary of the testing results:

a) Isolated testing was performed with only battery and only solar system where each of the power sources was coupled with our current and a new inverter. It was observed that our current inverter is optimized for our grid as it exhibits very short transient responses and stable steady state results.

b) The solar system is capable of producing power independently and is not the cause of the unusual behavior in Scenario 4 of Section 5. Hence, the original converter shall be maintained, even though the simulation does take significantly longer to run.

c) From testing of the isolated battery, it was found that one potential solution to prevent the load demand from dropping when the battery SOC is less than 20% is to manually control the charging current of the battery.

d) A promising result noticed was that the diesel generation system operates successfully in an isolated environment.

6.2 Lessons learned

A number of lessons learned during our project implementation in MATLAB Simulink and we wish to share them in the hope that they will be helpful for other researchers. The lessons are as follows.

a) Output from the original solar PV system was highly oscillated. By adding a controlled voltage source block (AC) and ramp function across the voltage terminals, we were able to stabilize the power output which is beneficial for the control system operation.

b) A stateflow logic is very appropriate for the fault interruption system as it can be replicated through microprocessor-based relays that are common in today power industry. We tried to use Simulink logic operator blocks but they were not suitable.

c) Simulation time is very long for our microgrid because it is complex with lots of components. Though, the use of Simulink "Rapid Accelerator" mode helps it run faster. Commenting out any unused calculation blocks, scopes, and closing graphs being plotted also help decrease simulation time. This is because the simulation time depends on the number of components in the project. The more the components, the longer it takes to simulate.

7. Conclusion

In this project, a load balancing scheme and a fault interruption system are developed and implemented to improve an autonomous microgrid design. These features are needed because they ensure satisfactory grid voltages by ensuring supply-demand balancing in more diverse situations while dealing with faulty conditions for the microgrid safety. These features were absent in the original microgrid design.

The load balancing scheme includes a modularized solar system, a dummy load, and an enhanced control system, aiming to maintain satisfactory voltages for the microgrid. The fault interruption system employs circuit breakers and a separate control system, aiming to extinguish fault currents timely to ensure the microgrid safety. The enhance microgrid is implemented using MATLAB Simulink.

The testing results have shown the following:

1) The control system works properly and can handle diverse operational situations, such as over- and under-power production of solar PV system, battery charge and discharge, and diesel generator activation.

2) The load balancing scheme is relatively effective in matching power supply with load demand using different power sources (solar PV system, battery, diesel generator). Voltage levels of both residential and commercial loads are maintained within a ±5% tolerance of their respective nominal values of 120V and 240V for all system-wide simulations.

3) The fault interruption system operates properly and is effective in dealing with various faulty conditions, such as single-line-to-ground, 2-line-to-ground, and permanent 3-line-to-ground faults. It successfully clears non-permanent faults and isolates a permanent fault.

Notably, the original microgrid has been improved to be more autonomous in the sense that it can deal with more diverse operational situations. It is much better protected by the newly-added fault interruption system. In terms of future work, further testing is desired to fix any abnormal behavior of the microgrid. Additionally, the relay system can be further improved upon by aligning more closely with best industry practices.

Overall, the study outcomes contribute to the expansion of smart autonomous microgrids as it has developed theoretical advanced features (supply-demand balancing and fault clearing) that are beneficial for real-world implementation of the microgrids. The implementation of additional intelligent microgrids, in turn, improves the dependability and resiliency of large power grids while making communities energy independent.

Appendix

Note: All other block parameters not listed here are provided in [1].

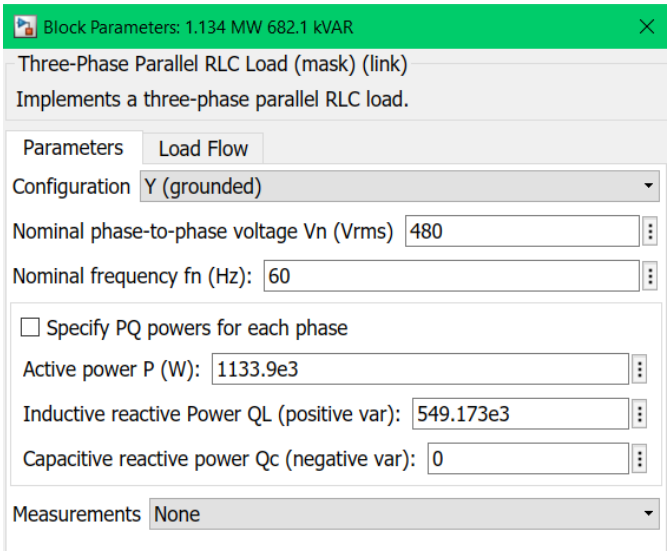

Fig. 36 Block parameters for three-phase loads

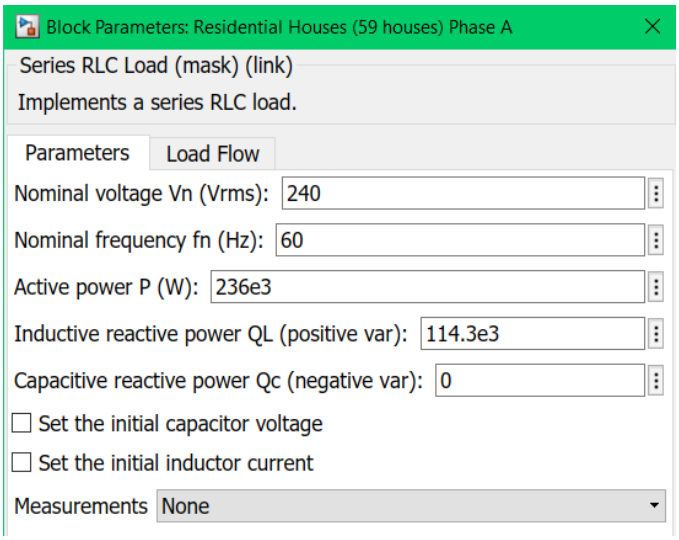

Fig. 37 Block parameters for single-phase loads

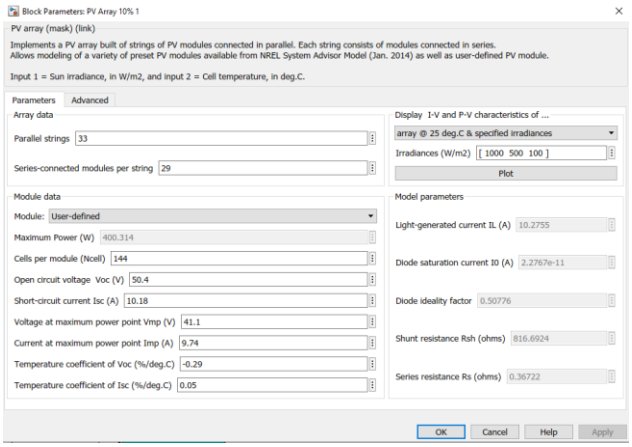

Fig. 38 Updated block parameters for PV Array (10% only)

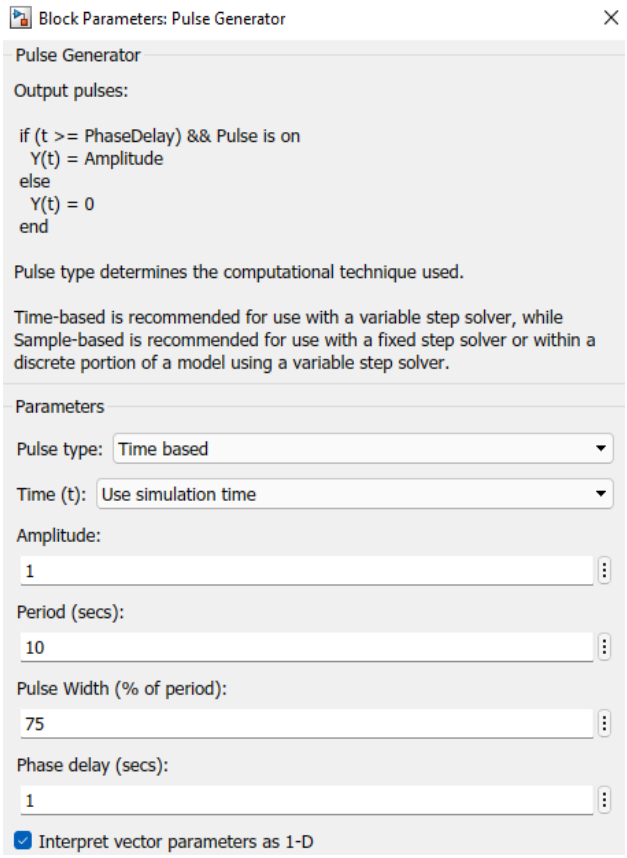

Fig. 39 Block parameters for temporary fault

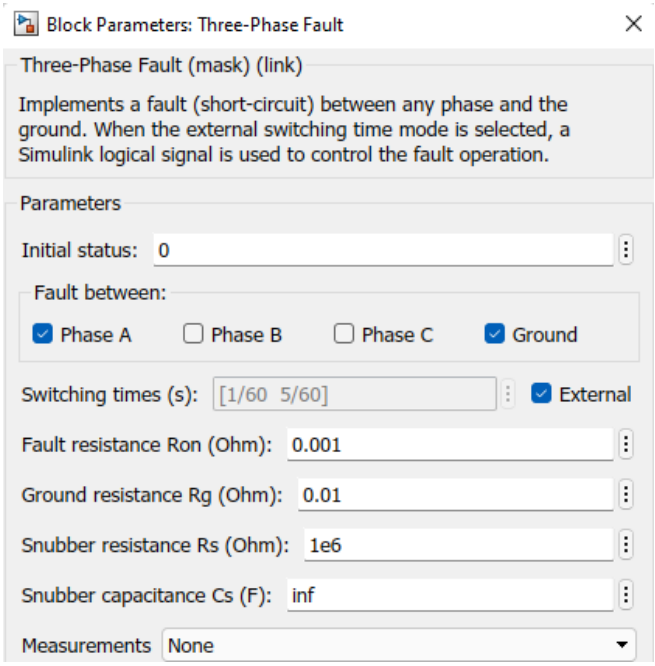

Fig. 40 Block parameters for SLG fault type

Acknowledgement

The student authors gratefully acknowledge and give thanks to Professor Ha Thu Le, our project advisor, for overseeing the project and providing consistent guidance and support throughout the 2021-2022 academic year. We greatly appreciate her patience and encouragement.

References

[1] H. N. Ho *et al.*, "Design and Simulation of an Autonomous Smart Microgrid for Energy Independence," *Wseas Transactions on Environment and Development*, vol. 17, pp. 911-928, 2021, doi: 10.37394/232015.2021.17.85.

[2] A. Muhtadi and A. M. Saleque, "Modeling and simulation of a microgrid consisting solar PV & DFIG based wind energy conversion system for St. Martin's island," presented at the 2017 IEEE 3rd International Conference on Engineering Technologies and Social Sciences (ICETSS), 2017/08, 2017. [Online]. Available: http://dx.doi.org/10.1109/icetss.2017.8324152 https://ieeexplore.ieee.org/document/8324152/.

[3] S. Santoso and H. T. Le, "Fundamental time-domain wind turbine models for wind power studies," *Elsevier Renewable Energy journal*, vol. 32, no. 14, pp. 2436-2452, 2007, doi: 10.1016/j.renere.2006.12.008.

[4] L. Zhang, B. Zhou, F. Cheng, and Y. Zhang, "Modeling and dynamic simulation of a novel doubly salient electro-magnetic wind power generator system," presented at the 2009 World Non-Grid-Connected Wind Power and Energy Conference, 2009/09, 2009. [Online]. Available: http://dx.doi.org/10.1109/wnwec.2009.5335781.

[5] D. V. Bozalakov, J. Laveyne, J. Desmet, and L. Vandevelde, "Overvoltage and voltage unbalance mitigation in areas with high penetration of renewable energy resources by using the modified three- phase damping control strategy," vol. 168, pp. 283-294, 2019, doi: 10.1016/j.epsr.2018.12.001.

[6] M. E. Khodayar, M. R. Feizi, and A. Vafamehr, "Solar photovoltaic generation: Benefits and operation challenges in distribution networks," *The Electricity Journal*, vol. 32, no. 4, pp. 50-57, 2019/05 2019, doi: 10.1016/j.tej.2019.03.004.

[7] S. Hashemi and J. Østergaard, "Methods and strategies for overvoltage prevention in low

voltage distribution systems with PV," *IET Renewable Power Generation*, vol. 11, no. 2, pp. 205-214, 2017/01/17 2017, doi: 10.1049/iet-rpg.2016.0277.

[8] X. Qin *et al.*, "Study of the application of active power adjustment and control technology based on modem energy storage into power system stability control and voltage adjustment," presented at the 2014 International Conference on Power System Technology, 2014/10, 2014. [Online]. Available: http://dx.doi.org/10.1109/powercon.2014.7194376 .

[9] W. Ma, W. Wang, X. Wu, R. Hu, F. Tang, and W. Zhang, "Control Strategy of a Hybrid Energy Storage System to Smooth Photovoltaic Power Fluctuations Considering Photovoltaic Output Power Curtailment," *Sustainability*, vol. 11, no. 5, p. 1324, 2019/03/03 2019, doi: 10.3390/su11051324.

[10] W. Ma *et al.*, "Optimal Allocation of Hybrid Energy Storage Systems for Smoothing Photovoltaic Power Fluctuations Considering the Active Power Curtailment of Photovoltaic," *IEEE Access*, vol. 7, pp. 74787-74799, 2019, doi: 10.1109/access.2019.2921316.

[11] R. Tonkoski, L. A. C. Lopes, and T. H. M. El-Fouly, "Coordinated Active Power Curtailment of Grid Connected PV Inverters for Overvoltage Prevention," *IEEE Transactions on Sustainable Energy*, vol. 2, no. 2, pp. 139-147, 2011/04 2011, doi: 10.1109/tste.2010.2098483.

[12] P. Bauwens and J. Doutreloigne, "Switch for the Optimization of Module Power by Reconfiguration of All Strings (SOMBRA): An Insulated Integrated Switch for a Reconfigurable Solar Panel," *Energies*, vol. 12, no. 21, p. 4179, 2019/11/01 2019, doi: 10.3390/en12214179.

[13] D. La Manna, V. Li Vigni, E. Riva Sanseverino, V. Di Dio, and P. Romano, "Reconfigurable electrical interconnection strategies for photovoltaic arrays: A review," *Renewable and Sustainable Energy Reviews*, vol. 33, pp. 412-426, 2014/05/01/ 2014, doi: https://doi.org/10.1016/j.rser.2014.01.070.

[14] P. R. Satpathy and R. Sharma, "Power and mismatch losses mitigation by a fixed electrical reconfiguration technique for partially shaded photovoltaic arrays," *Energy Conversion and Management*, vol. 192, pp. 52-70, 2019/07 2019, doi: 10.1016/j.enconman.2019.04.039.

[15] A. A. Z. Diab, H. M. Sultan, I. S. Mohamed, O. N. Kuznetsov, and T. D. Do, "Application of Different Optimization Algorithms for Optimal Sizing of PV/Wind/Diesel/Battery Storage Stand-Alone Hybrid Microgrid," *IEEE Access*, vol. 7, pp. 119223-119245, 2019, doi: 10.1109/access.2019.2936656.

[16] N. W. A. Lidula and A. D. Rajapakse, "Microgrids research: A review of experimental microgrids and test systems," *Renewable and Sustainable Energy Reviews*, vol. 15, no. 1, pp. 186-202, 2011/01 2011, doi: 10.1016/j.rser.2010.09.041.

[17] L. Wang, C.-S. Lam, and M.-C. Wong, "Hybrid Structure of Static Var Compensator and Hybrid Active Power Filter (SVC//HAPF) for Medium-Voltage Heavy Loads Compensation," *IEEE Transactions on Industrial Electronics*, vol. 65, no. 6, pp. 4432-4442, 2018/06 2018, doi: 10.1109/tie.2017.2772201.

[18] B. V. Rao, G. V. N. Kumar, M. R. Priya, and P. V. S. Sobhan, "Implementation of Static VAR Compensator for Improvement of Power System Stability," presented at the 2009 International Conference on Advances in Computing, Control, and Telecommunication Technologies, 2009/12, 2009. [Online]. Available: http://dx.doi.org/10.1109/act.2009.117.

[19] P. Flores, J. Dixon, M. Ortuzar, R. Carmi, P. Barriuso, and L. Moran, "Static Var Compensator and Active Power Filter With Power Injection Capability, Using 27-Level Inverters and Photovoltaic Cells," *IEEE Transactions on Industrial Electronics*, vol. 56, no. 1, pp. 130-138, 2009/01 2009, doi: 10.1109/tie.2008.927229.

[20] Elprocus. "Types of Faults and Effects in Electrical Power Systems." Elprocus. https://www.elprocus.com/what-are-the-different-types-of-faults-in-electrical-power-systems/ (accessed 2021).

[21] L. F. F. Gutierres, G. Cardoso, and G. Marchesan, "Recloser-fuse coordination protection for distributed generation systems: methodology and priorities for optimal disconnections," presented at the 12th IET International Conference on Developments in Power System Protection (DPSP 2014), 2014. [Online]. Available: http://dx.doi.org/10.1049/cp.2014.0141.

[22] *IEEE Guide for Automatic Reclosing of Circuit Breakers for AC Distribution and Transmission Lines*, 9780738172934. [Online]. Available: http://dx.doi.org/10.1109/ieeestd.2012.6232415

[23] A. Sang-Pil, K. Chul-Hwan, R. K. Aggarwal, and A. T. Johns, "An alternative approach to adaptive single pole auto-reclosing in high voltage transmission systems based on variable dead time control," *IEEE Transactions on Power Delivery*, vol. 16, no. 4, pp. 676-686, 2001, doi: 10.1109/61.956756.

[24] T. P. Murray and A. Jones, "Field trials of Cutout mounted reclosers on single-phase spur lines in ESB networks, Ireland," presented at the IEEE

PES T&D 2010, 2010. [Online]. Available: http://dx.doi.org/10.1109/tdc.2010.5484219.

[25] H. T. Le, "ECE 4875: Wind & Solar Power Systems Lecture Notes," ed: California State Polytechnic University, Pomona, 2021.

[26] P. G. E. Company, "Voltage Tolerance Boundary," ed.

[27] C. W. Cable, "BareNRG ACSR Aluminum Conductor," ed, 2016.

[28] "PVWatts Calculator." https://pvwatts.nrel.gov/ (accessed 2021).

[29] A. Smith, "Dura-Power XI: Commercial Electric," ed.

[30] S. Santoso, *Fundamentals of Electric Power Quality*. Austin, TX: CreateSpace, 2012.

[31] A. J. Allen and S. Santoso, "Modeling Distribution Overcurrent Protective Devices for Time-Domain Simulations," in *2007 IEEE Power Engineering Society General Meeting*, 24-28 June 2007 2007, pp. 1-6, doi: 10.1109/PES.2007.386156.

[32] U. S. E. I. Administration. "Frequently Asked Questions " https://www.eia.gov/tools/faqs/faq.php?id=97&t=3#:~:text=How%20much%20electricity%20does%20an,about%20893%20kWh%20per%20month (accessed 2022).

[33] P. Engineering. "Voltage sags and what to do about them." https://www.plantengineering.com/articles/voltage-sags-and-what-to-do-about-them/ (accessed 2022).